Numerical Heat Transfer, Part A: Applications: An International Journal of Computation and Methodology

Publication details, including instructions for authors and subscription information:
http://www.tandfonline.com/loi/unht20

Accelerated Bayesian Inference for the Estimation of Spatially Varying Heat Flux in a Heat Conduction Problem

Helcio R. B. Orlande [a], George S. Dulikravich [b], Markus Neumayer [c], Daniel Watzenig [c] & Marcelo J. Colaço [a]

[a] Department of Mechanical Engineering, Politecnica/COPPE, Federal University of Rio de Janeiro — UFRJ, Rio de Janeiro, RJ, Brazil

[b] Department of Mechanical and Materials Engineering, MAIDROC Lab, Florida International University, Miami, Florida, USA

[c] Institute of Electrical Measurement and Measurement Signal Processing, Graz University of Technology, Graz, Austria

To cite this article: Helcio R. B. Orlande, George S. Dulikravich, Markus Neumayer, Daniel Watzenig & Marcelo J. Colaço (2014) Accelerated Bayesian Inference for the Estimation of Spatially Varying Heat Flux in a Heat Conduction Problem, Numerical Heat Transfer, Part A: Applications: An International Journal of Computation and Methodology, 65:1, 1-25

To link to this article: http://dx.doi.org/10.1080/10407782.2013.812008

Numerical Heat Transfer, Part A, 65: 1–25, 2014

ISSN: 1040-7782 print/1521-0634 online
DOI: 10.1080/10407782.2013.812008

Taylor & Francis
Taylor & Francis Group

ACCELERATED BAYESIAN INFERENCE FOR THE ESTIMATION OF SPATIALLY VARYING HEAT FLUX IN A HEAT CONDUCTION PROBLEM

Helcio R. B. Orlande[1], George S. Dulikravich[2], Markus Neumayer[3], Daniel Watzenig[3], and Marcelo J. Colaço[1]

[1]*Department of Mechanical Engineering, Politecnica/COPPE, Federal University of Rio de Janeiro — UFRJ, Rio de Janeiro, RJ, Brazil*
[2]*Department of Mechanical and Materials Engineering, MAIDROC Lab, Florida International University, Miami, Florida, USA*
[3]*Institute of Electrical Measurement and Measurement Signal Processing, Graz University of Technology, Graz, Austria*

This article aims at the acceleration of an inverse heat transfer problem solution within the Bayesian framework. The physical problem involves a spatially varying heat flux, which can reach very large magnitudes in small regions, such as in the heating imposed by high-power lasers. The inverse problem of estimating the imposed heat flux is solved by using the Markov chain Monte Carlo method, with simulated transient temperature measurements. The solution of the inverse problem is based on a reduced model, which consists of an improved lumped formulation of a linearized version of the original nonlinear problem. Two different priors are considered for the sought heat flux, including a total variation density and a Gaussian density. The Gaussian prior is based on the physics of the heat conduction problem. Parameters appearing in both priors are also estimated as part of the inference problem in hyperprior models. The Delayed Acceptance Metropolis-Hastings (DAMH) Algorithm and the Enhanced Approximation Error Model (AEM) are applied with the objective to improve the accuracy of the inverse problem solution.

INTRODUCTION

Despite the fact that the inverse problem of estimating a boundary heat flux in a heat conduction problem has been dealt with for a long time through different solution techniques, it still remains a very challenging problem. Such is, especially, the case when fast transients are involved and/or the flux is imposed on small spots, thus presenting large spatial variations. For example, this is the situation when high power lasers are used to heat bodies and the imposed heat flux needs to be accurately quantified and/or controlled.

Received 5 May 2012; accepted 8 May 2013.
This work was supported by CNPq, CAPES and FAPERJ, Brazilian agencies for the fostering of science.

Address correspondence to Helcio R. B. Orlande, Department of Mechanical Engineering-POLI/COPPE, Federal University of Rio de Janeiro UFRJ, Cid. Universitária, Cx. Postal: 68503, Rio de Janeiro, RJ 21941-972, Brazil. E-mail: helcio@mecanica.coppe.ufrj.br

NOMENCLATURE

a,b,c	dimensions of the plate	$\bar{T}$	approximate average temperature across the plate, obtained with the surrogate model given by Eqs. (3*a*)–(3*f*)
C	volumetric heat capacity	T_c	solution of the complete model given by Eqs. (1*a*)–(1*h*)
C^*	volumetric heat capacity evaluated at temperature T^*	TV	total variation, Eq. (11*b*)
D	total number of measurements	$\mathbf{W}$	covariance matrix for the likelihood
i	index of volumes along the x direction	$\tilde{\mathbf{W}}$	covariance matrix for the modified likelihood in the approximation error model
I	number of volumes along the x direction	x,y,z	Cartesian spatial variables
j	index of volumes along the y direction	$\mathbf{Y}$	vector of measurements
J	number of volumes along the y direction	α	parameter for the total variation prior, Eq. (11*a*)
k	thermal conductivity	α_0, γ_0	centers of the Rayleigh distributions for α and γ, respectively
k^*	thermal conductivity evaluated at temperature T^*	$\boldsymbol{\varepsilon}$	model error
$\mathbf{P}$	vector of parameters	$\bar{\boldsymbol{\varepsilon}}$	mean of the model error
q	spatially dependent imposed heat flux at the surface $z=c$	$\boldsymbol{\Gamma}$	covariance matrix for the Gaussian prior
q_{est}	estimated heat flux at the surface $z=c$	γ	parameter for the Gaussian prior, Eq. (13)
q_{exa}	exact heat flux at the surface $z=c$	$\boldsymbol{\mu}$	vector of means for the Gaussian prior
T	approximate temperature obtained with the reduced model, Eqs. (7*a*) and (7*b*).		
t	time		
$\mathbf{T}$	vector of estimated temperatures		
$\bar{T}_c$	average temperature across the plate, obtained with the complete model, Eq. (2)		

In this article, we examine the use of the Markov chain Monte Carlo (MCMC) method within the Bayesian framework [1–7], for the estimation of a spatially varying heat flux. The inverse problem is then recast in the form of statistical inference from the posterior probability density, which is the model for the conditional probability distribution of the unknown parameters given the measurements. The measurement model incorporating the related uncertainties is called the likelihood, that is, the conditional probability of the measurements given the unknown parameters. The model for the unknowns, that reflects all the uncertainty of the parameters without the information conveyed by the measurements, is called the prior model [1]. The formal mechanism to combine the new information (measurements) with the previously available information (prior) is known as the Bayes' theorem. Therefore, the term Bayesian is often used to describe the statistical inversion approach, which is based on the following principles [1]: 1.) All variables included in the model are modeled as random variables; 2.) the randomness describes the degree of information concerning their realizations; 3.) the degree of information concerning these values is coded in probability distributions; and 4.) the solution of the inverse problem is the posterior probability distribution, from which distribution point estimates and other statistics can be computed.

The physical problem examined here involves three-dimensional transient heat conduction in a plate with temperature dependent properties. Therefore, the computation of the direct problem solution, needed for the solution of the inverse problem, is very time-consuming. Limitations are then imposed on the number of states of the

Markov chain that can be computed within a feasible time, which can make the use of the standard MCMC method impractical for the present application where the number of unknowns is large. One possible way to overcome such difficulties is to use model reduction or surrogate techniques, instead of the complete model, for the computation of the direct problem solution at each state of the Markov chain, like in references [8, 9]. Other examples of inverse problem solutions dealing with complicated mathematical formulations of the physical problems, as well as with reduced or surrogate models, can be found in references [10–18].

In this article, a reduced model is used for the solution of the inverse problem, which is based on a linear formulation and on partial lumping across the thickness of the plate, which is assumed to be sufficiently thin. The classical lumped formulation, where temperature gradients are neglected across the thickness of the plate, was shown to provide accurate results for several practical problems [19–24]. On the other hand, for cases dealing with large imposed fluxes and short transients, such as the one under analysis in this work, the temperature gradients across the thickness of the plate cannot be fully neglected. For such cases, the reduced model based on the improved lumped approach [25, 26], where temperature gradients are not neglected but taken into account in an approximate form, can provide quite accurate results [27].

Since reduced or surrogate models do not exactly reproduce the associated complete models, different approaches have been developed in order to improve the solution of inverse problems obtained with approximate forms of the original mathematical formulation. Among such approaches, we have the delayed acceptance Metropolis-Hastings (DAMH) algorithm [28] and the approximation error model (AEM) [1, 29–33]. In the DAMH algorithm, the Metropolis-Hastings (MH) algorithm [1–7] is regularly applied with the reduced model. If a proposal state is accepted with the reduced model, another test of Hastings is performed with the complete model, to finally decide if such proposal should be accepted or not. In this sense, the DAMH can be seen as two nested MH algorithms, where the outer MH loop acts as a filter to pre-evaluate proposal candidates with the reduced model. In the AEM approach, the statistical model of the approximation error is constructed from prior information and then represented as additional noise in the measurement model, for the solution of the inverse problem. It should be noted that there is a principle difference between the DAMH and the AEM approaches, as the AEM uses the posterior modified by the error of the reduced model, whereas the DAMH generates samples from the correct posterior. Such two approaches are examined here, with two prior distributions for the sought heat flux. A noninformative total variation prior is considered, as well as a Gaussian prior based on the physics of the problem. For both cases, hyperparameters modeled in terms of Rayleigh distributions are estimated as part of the inference problem [1]. These two priors, as well as the delayed acceptance Metropolis-Hastings algorithm and the approximation error model, are compared for three different spatial distributions of the imposed heat flux, as described next. Input data for the inverse analysis is obtained by means of numerical simulations.

PHYSICAL PROBLEM AND MATHEMATICAL FORMULATION

The physical problem examined here involves three-dimensional transient heat conduction in a plate with temperature dependent thermal conductivity, $k(T)$, and

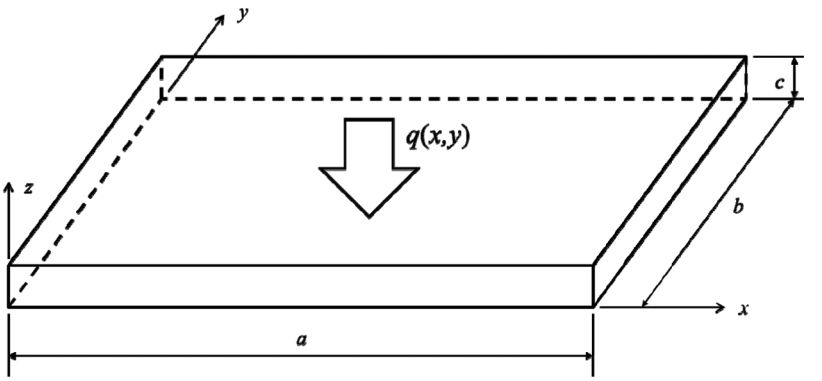

Figure 1. Physical problem.

volumetric heat capacity, $C(T)$, initially at a uniform temperature, T_0. The thickness of the plate, c, is assumed to be much smaller than its width, a, and length, b, so that heat transfer is neglected through the lateral boundaries. The plate bottom surface is assumed insulated, while a nonuniform heat flux $q(x,y)$ is imposed on its top surface (see Figure 1).

The mathematical formulation of this problem is given by the following.

$$C(T_c)\frac{\partial T_c(x,y,z,t)}{\partial t} = \frac{\partial}{\partial x}\left[k(T_c)\frac{\partial T_c}{\partial x}\right] + \frac{\partial}{\partial y}\left[k(T_c)\frac{\partial T_c}{\partial y}\right] + \frac{\partial}{\partial z}\left[k(T_c)\frac{\partial T_c}{\partial z}\right] \quad (1a)$$

$$\text{in } 0 < x < a, 0 < y < b, 0 < z < c, \text{ for } t > 0$$

$$\frac{\partial T_c}{\partial x} = 0 \text{ at } x = 0 \text{ and } x = a, 0 < y < b, 0 < z < c, \text{ for } t > 0 \quad (1b,c)$$

$$\frac{\partial T_c}{\partial y} = 0 \text{ at } y = 0 \text{ and } y = b, 0 < x < a, 0 < z < c, \text{ for } t > 0 \quad (1d,e)$$

$$\frac{\partial T_c}{\partial z} = 0 \text{ at } z = 0, 0 < x < a, 0 < y < b, \text{ for } t > 0 \quad (1f)$$

$$k(T_c)\frac{\partial T_c}{\partial z} = q(x,y) \text{ at } z = c, 0 < x < a, 0 < y < b, \text{ for } t > 0 \quad (1g)$$

$$T_c = T_0 \text{ for } t = 0, \text{ in } 0 < x < a, 0 < y < b, 0 < z < c \quad (1h)$$

Where the subscript c refers to the complete model, defined here as the one that perfectly reproduces all the phenomena of the physical problem, which is assumed to be exact within the accuracy of the numerical method used for its solution.

The average temperature across the thickness of the plate is defined by the following.

$$\bar{T}_c(x,y,t) = \frac{1}{c}\int_{z=0}^{c} T_c(x,y,z,t)\,dz \tag{2}$$

REDUCED MODEL FOR THE DIRECT PROBLEM

In this section, we introduce the reduced model used to approximate the physical problem described above. The reduced model involves partial lumping [19–27] along the z direction, since the plate is assumed to be thin, that is, $c \ll a$ and $c \ll b$. In addition, the reduced model is based on a linear approximation of problem (1a)–(1h), where the physical properties are evaluated at a temperature T^*. At this temperature, representative values C^* and k^* are obtained for the volumetric heat capacity and thermal conductivity within the plate, respectively. The solution of the linearized version of problem (1a)–(1h) is denoted $T(x, y, z, t)$.

By operating on Eqs. (1a)–(1e) and (1h) with $\frac{1}{c}\int_{z=0}^{c}(\cdot)\,dz$, making use of the boundary conditions (1f) and (1g), at $z = 0$ and $z = c$, respectively, and assuming constant thermophysical properties, the following problem is obtained for the computation of the approximate average temperature $\bar{T}(x,y,t)$.

$$C^* \frac{\partial \bar{T}(x,y,t)}{\partial t} = \frac{\partial}{\partial x}\left[k^* \frac{\partial \bar{T}}{\partial x}\right] + \frac{\partial}{\partial y}\left[k^* \frac{\partial \bar{T}}{\partial y}\right] + \frac{q(x,y)}{c} \quad \text{in } 0 < x < a,\ 0 < y < b, \text{ for } t > 0 \tag{3a}$$

$$\frac{\partial \bar{T}}{\partial x} = 0 \quad \text{at } x = 0 \quad \text{and} \quad x = a, \quad 0 < y < b, \text{ for } t > 0 \tag{3b,3c}$$

$$\frac{\partial \bar{T}}{\partial y} = 0 \quad \text{at } y = 0 \quad \text{and} \quad y = b, \quad 0 < x < a, \text{ for } t > 0 \tag{3d,3e}$$

$$\bar{T} = T_0 \quad \text{for } t = 0, \text{ in } 0 < x < a,\ 0 < y < b \tag{3f}$$

where

$$\bar{T}(x,y,t) = \frac{1}{c}\int_{z=0}^{c} T(x,y,z,t)\,dz \tag{4}$$

Surface temperature measurements are assumed to be available for the inverse analysis, as will be further discussed below. Therefore, from the first level of approximation, where the temperature $\bar{T}(x,y,t)$ is obtained as a solution of problem (3a)–(3f) and used in place of the actual average temperature $\bar{T}_c(x,y,t)$, several reduced models can be derived. These reduced models differ in terms of how $\bar{T}(x,y,t)$ relates to the surface temperatures at $z = 0$ and $z = c$.

In the *classical lumped formulation* [19–27], temperature gradients across the thickness of the plate are fully neglected. Therefore, the surface temperatures become equal to the average temperature; that is,

$$T(x,y,0,t) = T(x,y,c,t) = \bar{T}(x,y,t) \qquad (5a,b)$$

In the *improved lumped formulation* based on the coupled integral equations Approach [25–27], the temperature gradients across the thickness of the plate are not neglected, but taken into account in an approximate form, which can involve different degrees of accuracy. Here, we use the so-called $H_{1,1}/H_{0,0}$ approximation [25], where the Hermite's formulae $H_{1,1}$ and $H_{0,0}$ are applied to approximate the average temperature $\bar{T}(x,y,t)$ and the integral of the temperature gradient along the z direction, respectively. The $H_{1,1}$ formula (corrected trapezoidal rule), as applied to the definition of the approximate average temperature (4), is given by the following [25].

$$\bar{T}(x,y,t) \approx \frac{1}{2}[T(x,y,0,t) + T(x,y,c,t)] + \frac{c}{12}\left[\left.\frac{\partial T}{\partial z}\right|_{z=0} - \left.\frac{\partial T}{\partial z}\right|_{z=c}\right] \qquad (6a)$$

The $H_{0,0}$ formula (trapezoidal rule) is now applied to the integral of the temperature gradient [25]; that is,

$$\int_{z=0}^{c} \frac{\partial T(x,y,z,t)}{\partial z}\, dz = T(x,y,c,t) - T(x,y,0,t) \approx \frac{c}{2}\left[\left.\frac{\partial T}{\partial z}\right|_{z=0} + \left.\frac{\partial T}{\partial z}\right|_{z=c}\right] \qquad (6b)$$

Equations (6*a*), and (6*b*) are then solved, together with boundary conditions (1*f*), and (1*g*) with constant thermophysical properties, to yield the following relations between the surface temperatures and the approximate average temperature.

$$T(x,y,0,t) = \bar{T}(x,y,t) - \frac{c}{6k^*} q(x,y) \qquad (7a)$$

$$T(x,y,c,t) = \bar{T}(x,y,t) + \frac{c}{3k^*} q(x,y) \qquad (7b)$$

We note from Eqs. (5) and (7) that the computational efforts for the classical and for the improved lumped formulations are practically the same. Differences between these efforts are limited to algebraic operations required to compute $T(x, y, 0, t)$ and $T(x, y, c, t)$ with Eqs. (7*a*), and (7*b*), which can actually be done as post-processing to the solution of problem (3*a–f*). On the other hand, much more accurate solutions are indeed obtained with the improved lumped formulation for the kind of physical problem examined here [27], since the temperature gradients are not neglected as in the classical lumped formulation.

INVERSE PROBLEM

The inverse problem of interest in this paper is concerned with the estimation of the boundary heat flux $q(x,y)$, by using transient temperature measurements taken at the bottom surface, $z = 0$. The measurements are assumed to be taken with an infrared camera. Such measurement technique is quite powerful, because it can provide accurate nonintrusive measurements, with fine spatial resolutions and at large frequencies [7, 19–24, 26].

For the inverse analysis, the unknown function $q(x,y)$ is discretized spatially at the plate surface. The discretized flux is considered uniform over a grid with center points (x_i, y_j), where $x_i = i\Delta x$, $y_j = j\Delta y$, $i = 1, \ldots, I$, $j = 1, \ldots, J$, and with grid spacing given by $\Delta x = a/I$ and $\Delta y = b/J$. Therefore, the function is estimated in terms of its local values, which are suitably arranged in a vector of unknown parameters here denoted as $\mathbf{P}$. For the sake of simplicity, the transient temperature measurements are also assumed to be available over this same grid. Therefore, the local measurements may actually result from some spatial averaging of the readings obtained with the infrared camera, if it is capable of providing a resolution more refined than that used in the domain discretization. The transient measurements at each grid point (x_i, y_j) and each time step are also arranged in a vector, here denoted as $\mathbf{Y}$.

We apply the Markov chain Monte Carlo (MCMC) method to obtain estimates of the posterior distribution of the unknown heat flux components, within the Bayesian framework [1–7]. Bayes' theorem is stated as follows [1–7].

$$\pi_{posterior}(\mathbf{P}) = \pi(\mathbf{P}|\mathbf{Y}) = \frac{\pi(\mathbf{P})\pi(\mathbf{Y}|\mathbf{P})}{\pi(\mathbf{Y})} \tag{8}$$

Where $\pi_{posterior}(\mathbf{P})$ is the posterior probability density, $\pi(\mathbf{P})$ is the prior density, $\pi(\mathbf{Y}|\mathbf{P})$ is the likelihood function, and $\pi(\mathbf{Y})$ is the marginal probability density of the measurements, which plays the role of a normalizing constant.

The most common MCMC algorithm is the one due to Metropolis and Hastings [1–7]. The implementation of the Metropolis-Hastings algorithm starts with the selection of a proposal distribution $p(\mathbf{P}^*, \mathbf{P}^{(t-1)})$ which is used to draw a new candidate state $\mathbf{P}^*$, given the current state $\mathbf{P}^{(t-1)}$ of the Markov chain. Once this jumping distribution has been selected, the Metropolis-Hastings algorithm can be implemented by repeating the following steps.

Step 1. Sample a candidate point $\mathbf{P}^*$ from a proposal distribution $p(\mathbf{P}^*, \mathbf{P}^{(t-1)})$.
Step 2. Calculate the acceptance factor:

$$\alpha = \min\left[1, \frac{\pi(\mathbf{P}^*|\mathbf{Y})\, p(\mathbf{P}^{(t-1)}, \mathbf{P}^*)}{\pi(\mathbf{P}^{(t-1)}|\mathbf{Y})\, p(\mathbf{P}^*, \mathbf{P}^{(t-1)})}\right] \tag{9}$$

Step 3. Generate a random value U that is uniformly distributed on]0,1[.
Step 4. If $U \leq \alpha$, set $\mathbf{P}^{(t)} = \mathbf{P}^*$; otherwise, set $\mathbf{P}^{(t)} = \mathbf{P}^{(t-1)}$.
Step 5. Return to Step 1.

In this way, a sequence is generated to represent the posterior distribution and inference on this distribution is obtained from inference on the samples $\{\mathbf{P}^{(1)}, \mathbf{P}^{(2)}, \ldots, \mathbf{P}^{(n)}\}$. We note that values of $\mathbf{P}^{(i)}$ must be ignored while the chain has not converged to equilibrium (the burn-in period).

By assuming that the measurement errors are Gaussian random variables, with zero means and known covariance matrix $\mathbf{W}$ and that the measurement errors are additive and independent of the parameters $\mathbf{P}$, the likelihood function can be expressed as follows [1–7].

$$\pi(\mathbf{Y}|\mathbf{P}) = (2\pi)^{-D/2}|\mathbf{W}|^{-1/2}\exp\left\{-\frac{1}{2}[\mathbf{Y}-\mathbf{T}(\mathbf{P})]^T\mathbf{W}^{-1}[\mathbf{Y}-\mathbf{T}(\mathbf{P})]\right\} \tag{10}$$

Where D is the total number of measurements, and $\mathbf{T}(\mathbf{P})$ is the solution of the direct problem at the specific times and locations of each measurement. Here, the direct problem solution is obtained from the improved lumped formulation described above, with known $\mathbf{P}$.

Two different prior densities are examined for the spatially distributed heat flux. One of these densities is a total variation non-informative prior [1]. It is a Markov random field, capable of accurately estimating the sought spatially distributed function [1]. The total variation prior is given in the following form:

$$\pi(\mathbf{P}) \propto \exp[-\alpha\, TV(\mathbf{P})] \tag{11a}$$

Where, for the present case,

$$\begin{aligned} TV(\mathbf{P}) = \sum_{i=2}^{I-1}\sum_{j=2}^{J-1} \Delta y\big[\big|q(x_i,y_j)-q(x_{i+1},y_j)\big| + \big|q(x_i,y_j)-q(x_{i-1},y_j)\big|\big] + \\ + \Delta x\big[\big|q(x_i,y_j)-q(x_i,y_{j+1})\big| + \big|q(x_i,y_j)-q(x_i,y_{j-1})\big|\big] \end{aligned} \tag{11b}$$

The other prior density examined in this work is Gaussian and based on a model of very low accuracy that still takes into account the physics of the problem. In order to generate the prior, we consider a finite control volume at the same grid used for the heat flux, that is, with grid spacing given by $\Delta x = a/I$ and $\Delta y = b/J$, as illustrated by Figure 2. It is assumed that the temperature inside such control volume is uniform, that is, the lumped formulation is valid. If heat transfer is neglected through all the boundaries of this discrete control volume, except through the top surface where the heat flux $q(x_i, y_j)$ is imposed, the following relation results from the energy balance.

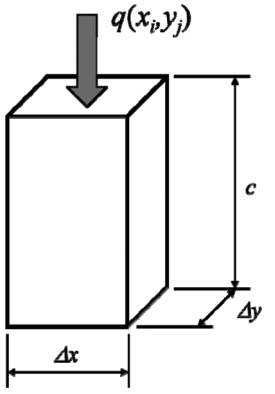

Figure 2. Finite control volume used to obtain the Gaussian prior.

$$q(x_i, y_j) = C^* c \frac{d\,T(x_i, y_j)}{d\,t} \tag{12}$$

That is, the local imposed heat flux is proportional to the local rate of temperature increase. Clearly, if the local rate of temperature increase can be somehow estimated, an estimate can be obtained for $q(x_i, y_j)$ that might be appropriate to be used as prior information for the sought heat flux. In order to generate this physically motivated Gaussian prior, and at the same time not violate the Bayesian principle that the prior is the information for the unknowns (coded in the form of probability distribution functions) that is available before the measurements are taken, we assume here that another kind of measurements is also available. Such other kind of measurements is only used to generate the prior, and is considered independent of the temperature measurements used in the inverse analysis, that is, for the computation of the likelihood. This other type of measurement (let us say, V) is related to the local temperature increase through some linear relation $\Delta V \propto \Delta T$, where Δ denotes variation, so that the local heat flux can be calculated with Eq. (12), at each time step. The local Gaussian distributions were then based on the means and variances of the heat fluxes calculated at each time step. Anyhow, the linear dependences of such means and variances of the applied heat flux and of the measurements were neglected, for the application of the MCMC method.

Let us denote the vector containing the means of each local heat flux as $\boldsymbol{\mu}$ and the associated covariance matrix as $\boldsymbol{\Gamma}$. The Gaussian prior is then given by the following.

$$\pi(\mathbf{P}) = \frac{\gamma^{IJ/2}}{\sqrt{(2\pi)^{IJ}|\boldsymbol{\Gamma}|}} \exp\left[-\frac{1}{2}\gamma(\mathbf{P}-\boldsymbol{\mu})^T\boldsymbol{\Gamma}^{-1}(\mathbf{P}-\boldsymbol{\mu})\right] \tag{13}$$

Where the parameter γ was introduced in Eq. (13) in order to take into account that the means $\boldsymbol{\mu}$ and the covariance matrix $\boldsymbol{\Gamma}$ are poorly known, since they were obtained with the very simplified model used to the generate the Gaussian prior, as described above.

The parameters α and γ, appearing in the total variation and Gaussian priors, respectively, are treated in this work as hyperparameters; that is, they are estimated as part of the inference problem in a hierarchical model [1]. The hyperprior densities for these parameters are taken in the form of Rayleigh distributions. Therefore, the posterior distributions, based on the total variation and Gaussian priors, are given, respectively, by the following.

$$\pi(\alpha, \mathbf{P}|\mathbf{Y}) \propto \alpha \exp\left\{-\frac{1}{2}[\mathbf{Y}-\mathbf{T}(\mathbf{P})]^T\mathbf{W}^{-1}[\mathbf{Y}-\mathbf{T}(\mathbf{P})] - \alpha\, TV(\mathbf{P}) - \frac{1}{2}\left(\frac{\alpha}{\alpha_0}\right)^2\right\} \tag{14a}$$

$$\pi(\gamma, \mathbf{P}|\mathbf{Y}) \propto \gamma^{(IJ+2)/2} \exp\left\{-\frac{1}{2}[\mathbf{Y}-\mathbf{T}(\mathbf{P})]^T\mathbf{W}^{-1}[\mathbf{Y}-\mathbf{T}(\mathbf{P})] - \frac{1}{2}\gamma(\mathbf{P}-\mu)^T\boldsymbol{\Gamma}^{-1}(\mathbf{P}-\mu) - \frac{1}{2}\left(\frac{\gamma}{\gamma_0}\right)^2\right\} \tag{14b}$$

Where $\alpha_0 > 0$ and $\gamma_0 > 0$ are the center points of the Rayleigh distributions.

Since the reduced model, given by the improved lumped formulation of Eqs. (7*a*) and (7*b*), does not exactly reproduce the solution of the complete model

given by Eqs. (1*a*–1*h*), two approaches are used here in an attempt to improve the accuracy of the inverse problem solution. Such approaches are described next.

DELAYED ACCEPTANCE METROPOLIS-HASTINGS ALGORITHM

In the delayed acceptance Metropolis-Hastings (DAMH) algorithm [28], the regular Metropolis-Hastings algorithm, presented in the section above, is applied with the reduced model for the computation of the likelihood function. If a proposal state is accepted, then another test of Hastings is performed with the complete model, to finally decide if such proposal should be accepted or not. The DAMH algorithm can be summarized as follows [28].

Step 1. Sample a candidate point $\mathbf{P}^*$ from a proposal distribution $p(\mathbf{P}^*, \mathbf{P}^{(t-1)})$.
Step 2. Calculate the acceptance factor with the reduced model.

$$\alpha = \min\left[1, \frac{\pi(\mathbf{P}^*|\mathbf{Y})\, p(\mathbf{P}^{(t-1)}, \mathbf{P}^*)}{\pi(\mathbf{P}^{(t-1)}|\mathbf{Y})\, p(\mathbf{P}^*, \mathbf{P}^{(t-1)})}\right] \tag{15a}$$

Step 3. Generate a random value U that is uniformly distributed on]0,1[.
Step 4. If $U \leq \alpha$, proceed to step 5. Otherwise, return to step 1.
Step 5. Calculate a new acceptance factor with the complete model.

$$\alpha_c = \min\left[1, \frac{\pi_c(\mathbf{P}^*|\mathbf{Y})\, p(\mathbf{P}^{(t-1)}, \mathbf{P}^*)}{\pi_c(\mathbf{P}^{(t-1)}|\mathbf{Y})\, p(\mathbf{P}^*, \mathbf{P}^{(t-1)})}\right] \tag{15b}$$

Step 6. Generate a new random value U_c which is uniformly distributed on]0,1[.
Step 7. If $U_c \leq \alpha_c$, set $\mathbf{P}^{(t)} = \mathbf{P}^*$. Otherwise, set $\mathbf{P}^{(t)} = \mathbf{P}^{(t-1)}$.
Step 8. Return to Step 1.

Where $\pi(\mathbf{P}|\mathbf{Y})$and $\pi_c(\mathbf{P}|\mathbf{Y})$ are the posterior distributions with the likelihoods computed with the reduced model and with the complete model, respectively.

With the DAMH algorithm, it is expected to take advantage of the fast computations of the reduced model in order to find, in step 4, possible candidates to be accepted with the complete model, in step 7. The DAMH algorithm can be quite effective, especially in the case of a low acceptance ratio of the MH algorithm. Therefore, depending on how fast the solution of the reduced model is as compared to that of the complete model, as well as on the acceptance ratio, the use of the DAMH algorithm might result in significant reductions in computational times, as compared to those from the regular MH algorithm applied to the complete model.

APPROXIMATION ERROR MODEL

In the approximation error model (AEM) approach, the statistical model of the approximation error is constructed and then represented as additional noise in the measurement model [1, 29–33]. With the hypotheses that the measurement errors are additive and independent of the parameters $\mathbf{P}$, one can write the following.

$$\mathbf{Y} = \mathbf{T}_c(\mathbf{P}) + \mathbf{e} \tag{16}$$

Where $\mathbf{T}_c(\mathbf{P})$ is the sufficiently accurate solution of the complete model given by Eqs. (1*a*)–(1*h*). The vector of measurement errors, $\mathbf{e}$, are assumed here to be Gaussian, with zero mean and known covariance matrix $\mathbf{W}$, so that the likelihood function is given by Eq. (10).

In this article, the solution of the reduced model, $\mathbf{T}(\mathbf{P})$, given by Eqs. (3*a*)–(3*f*), (7*a*), and (7*b*), is used for the solution of the inverse problem, in place of the solution of the complete model, $\mathbf{T}_c(\mathbf{P})$. Thus, Eq. (16) becomes the following.

$$\mathbf{Y} = \mathbf{T}(\mathbf{P}) + [\mathbf{T}_c(\mathbf{P}) - \mathbf{T}(\mathbf{P})] + \mathbf{e} \tag{17}$$

By defining the error between the complete and the reduced model solutions as,

$$\boldsymbol{\varepsilon}(\mathbf{P}) = [\mathbf{T}_c(\mathbf{P}) - \mathbf{T}(\mathbf{P})] \tag{18}$$

Eq. (17) can be written as follows.

$$\mathbf{Y} = \mathbf{T}(\mathbf{P}) + \boldsymbol{\eta}(\mathbf{P}) \tag{19}$$

where,

$$\boldsymbol{\eta}(\mathbf{P}) = \boldsymbol{\varepsilon}(\mathbf{P}) + \mathbf{e} \tag{20}$$

One difficult with such an approach is to model the error $\boldsymbol{\eta}(\mathbf{P})$, which includes the direct problem solution errors, $\boldsymbol{\varepsilon}(\mathbf{P})$, as well as the experimental errors, $\mathbf{e}$. A simple, but very effective approximation error approach, is to model such an error as a Gaussian variable [1, 29–33]. Another important point for the implementation of the approximation error model is that the statistics of $\boldsymbol{\eta}(\mathbf{P})$, like its mean and covariance matrix, are based on the prior distribution [1, 29–33]. Since smoothness priors, such as the total variation prior given by Eqs. (11*a*) and (11*b*), are improper; that is, their variances are unbound, only the Gaussian prior given by Eq. (13) is then used in this paper for the approximation error model approach [1, 29–33].

Therefore, with the approximation error model approach, the posterior Eq. (14*b*) is rewritten as follows [29].

$$\tilde{\pi}(\gamma, \mathbf{P}|\mathbf{Y}) \propto \gamma^{(IJ+2)/2} \exp\left\{ -\frac{1}{2}[\mathbf{Y} - \mathbf{T}(\mathbf{P}) - \bar{\boldsymbol{\eta}}]^T \tilde{\mathbf{W}}^{-1} [\mathbf{Y} - \mathbf{T}(\mathbf{P}) - \bar{\boldsymbol{\eta}}] - \frac{1}{2}\gamma(\mathbf{P} - \boldsymbol{\mu})^T \boldsymbol{\Gamma}^{-1}(\mathbf{P} - \boldsymbol{\mu}) - \frac{1}{2}\left(\frac{\gamma}{\gamma_0}\right)^2 \right\} \tag{21}$$

where,

$$\bar{\boldsymbol{\eta}} = \bar{\boldsymbol{\varepsilon}} + \bar{\mathbf{e}} + \boldsymbol{\Gamma}_{\boldsymbol{\eta}\mathbf{P}} \boldsymbol{\Gamma}^{-1}(\mathbf{P} - \boldsymbol{\mu}) \tag{22a}$$

$$\tilde{\mathbf{W}} = \mathbf{W}_{\boldsymbol{\varepsilon}} + \mathbf{W} - \boldsymbol{\Gamma}_{\boldsymbol{\eta}\mathbf{P}} \boldsymbol{\Gamma}^{-1} \boldsymbol{\Gamma}_{\mathbf{P}\boldsymbol{\eta}} \tag{22b}$$

$\bar{\boldsymbol{\varepsilon}}$ and $\bar{\mathbf{e}}$ are the means of $\boldsymbol{\varepsilon}$ and $\mathbf{e}$, respectively, while $\mathbf{W}_{\varepsilon}$ is the covariance of $\boldsymbol{\varepsilon}$, and $\boldsymbol{\Gamma}_{\boldsymbol{\eta}\mathbf{P}}$ is the covariance of $\boldsymbol{\eta}$ and $\mathbf{P}$, respectively. Equations (22*a*) and (22*b*) give the complete error model [29]. We note that, with the standard hypotheses regarding

the measurement errors made above, $\bar{\mathbf{e}} = 0$. By further neglecting the dependency of $\boldsymbol{\eta}$ and $\mathbf{P}$, that is, $\boldsymbol{\Gamma}_{\boldsymbol{\eta}\mathbf{P}} = 0$, Eqs. (22*a*) and (22*b*) simplify to the so-called enhanced error model that is used here, given by the following [29].

$$\bar{\boldsymbol{\eta}} \approx \bar{\boldsymbol{\varepsilon}} \tag{23a}$$

$$\tilde{\mathbf{W}} \approx \mathbf{W}_{\boldsymbol{\varepsilon}} + \mathbf{W} \tag{23b}$$

RESULTS AND DISCUSSIONS

For all cases examined below, the plate was assumed to be made of stainless steel with dimensions $a = 0.12\,\text{m}$, $b = 0.12\,\text{m}$, $c = 0.003\,\text{m}$, and with the following properties.

$$C(T) = 1,324.75T + 3,557,900 \tag{24a}$$

$$k(T) = 12.45 + 0.014T + 2.517\text{x}10^{-6}T^2 \tag{24b}$$

Where the units of temperature, volumetric heat capacity and thermal conductivity in Eqs. (24*a*) and (24*b*) are K, $\text{Jm}^{-3}\text{K}^{-1}$ and $\text{Wm}^{-1}\text{K}^{-1}$, respectively. The plate was assumed to be initially at the uniform temperature $T_0 = 300\,\text{K}$.

The components $q(x_i, y_j)$ of the discretized heat flux were sought over a grid with $\Delta x = \Delta y = 0.005\,\text{m}$, that is, $I = J = 24$. The solutions of the complete model, given by Eqs. (1*a*)–(1*h*), and of the reduced model, given by Eqs. (3*a*)–(3*f*), were obtained by finite volumes. The complete model was discretized with $\Delta x = \Delta y = 0.005\,\text{m}$ and $\Delta z = 0.0005\,\text{m}$, while the reduced model was discretized with $\Delta x = \Delta y = 0.005\,\text{m}$. For the two models, the systems resulting from the finite volume discretization were integrated explicitly in time, with a time step $\Delta t = 0.01\,\text{s}$. The final time was fixed at 2 s. The constant thermophysical properties used in the reduced model were obtained from Eqs. (15*a*) and (15*b*) at $T^* = 600\,\text{K}$.

Computational times in this work were obtained using the Matlab platform, on a computer with an Intel i5 CPU and 4 GB of RAM. In general, the direct problem solution with the complete model took around 7.2 s, while the solution with the reduced model in the form of the improved lumped approach given by Eqs. (7*a*) and (7*b*), took around 0.09 s of computational time. This clearly demonstrates the necessity of a reduced model for the solution of the inverse problem with the MCMC method in the present case. In fact, if we consider 100,000 states of the Markov chain, the solution of the direct problem alone with the complete model would require at least eight days of computation. On the other hand, with the reduced model the required computational time reduces to around 2.5 h.

Three different heat flux functions were examined in this work, involving sharp discontinuities and heat fluxes of large magnitudes; they were selected in order to challenge the inverse problem solution procedure with each prior distribution, as well as with either the delayed acceptance Metropolis-Hastings algorithm (DAMH) algorithm or the approximation error model (AEM) approach. These functions are denoted as flux A (with two small heating spots), flux B (with one single small

heating spot), and flux C (with one single large heating spot). They are defined as follows.

$$\textbf{Flux A:}\ q(x_i, y_j) = \begin{cases} 10^7\ \mathrm{Wm}^{-2} & , \quad \text{for } 8 \le i \le 10 \quad \text{and} \quad 8 \le j \le 10 \\ 10^7\ \mathrm{Wm}^{-2} & , \quad \text{for } 18 \le i \le 20 \quad \text{and} \quad 18 \le j \le 20 \\ 0 & \text{elsewhere} \end{cases} \tag{25a}$$

$$\textbf{Flux B:}\ q(x_i, y_j) = \begin{cases} 10^7\ \mathrm{Wm}^{-2} & , \quad \text{for } 8 \le i \le 10 \quad \text{and} \quad 8 \le j \le 10 \\ 0 & \text{elsewhere} \end{cases} \tag{25b}$$

$$\textbf{Flux C:}\ q(x_i, y_j) = \begin{cases} 10^7\ \mathrm{Wm}^{-2} & , \quad \text{for } 8 \le i \le 15 \quad \text{and} \quad 8 \le j \le 15 \\ 0 & \text{elsewhere} \end{cases} \tag{25c}$$

where $1 \le i \le I = 24$ and $1 \le j \le J = 24$.

Figures 3*a*–3*c* present the temperature distributions at the bottom ($z = 0$) and top ($z = c$) surfaces computed with the complete model given by Eqs. (1*a*)–(1*h*), at time $t = 1.9$ s, for heat fluxes A–C, respectively. These figures clearly show the very large temperature gradients across the plate, as well as along the x and y directions, resulting from the large magnitudes of the applied heat flux at small spots.

For the solution of the inverse problem, the simulated temperature measurements were given at $z = 0$, also over the grid with $\Delta x = \Delta y = 0.005$ m, at every $\Delta t = 0.01$ s. The simulated measurements were generated from the solution of the complete model given by Eqs. (1*a*)–(1*h*). Uncorrelated errors with a Gaussian distribution, zero mean and two different levels of a constant standard deviation were then added to the solution of the complete model to simulate actual measurements. The two standard deviations applied for the simulated measurements were 0.02 K and 1.25 K. The lower value of the standard deviation is typical of nowadays accurate infrared cameras, which are mainly used in laboratory measurements [7, 19–24]. The larger value of the standard deviation was selected to challenge the techniques examined in this paper, in special for field applications where low-accuracy infrared cameras are commonly used.

The test cases examined here, involving the different priors and approaches to improve the accuracy of the inverse problem solution that were described above, are summarized in Table 1. The TV prior was used for test cases 1–6. The regular Metropolis-Hasting algorithm was applied for test cases 1–3 by using the reduced model for the direct problem, but the delayed acceptance Metropolis-Hasting algorithm was applied for test cases 4–6. Test cases 7–12 are based on the Gaussian prior. While the regular Metropolis-Hastings algorithm based only on the reduced model was used for test cases 7–9, the enhanced error model approach was used for test cases 10–12.

For the AEM approach (cases 10–12), the parameters of the Gaussian distribution that is proposed for the modeling error (see Eqs. (19)–(23), were quantified as follows. The local heat flux was calculated with Eq. (12) at each time step, by using the local temperature increase rate computed with the second set of measurements v, as discussed above. This other type of measurements used to generate the prior was simulated with larger standard deviations for their errors, that is, the equivalent of

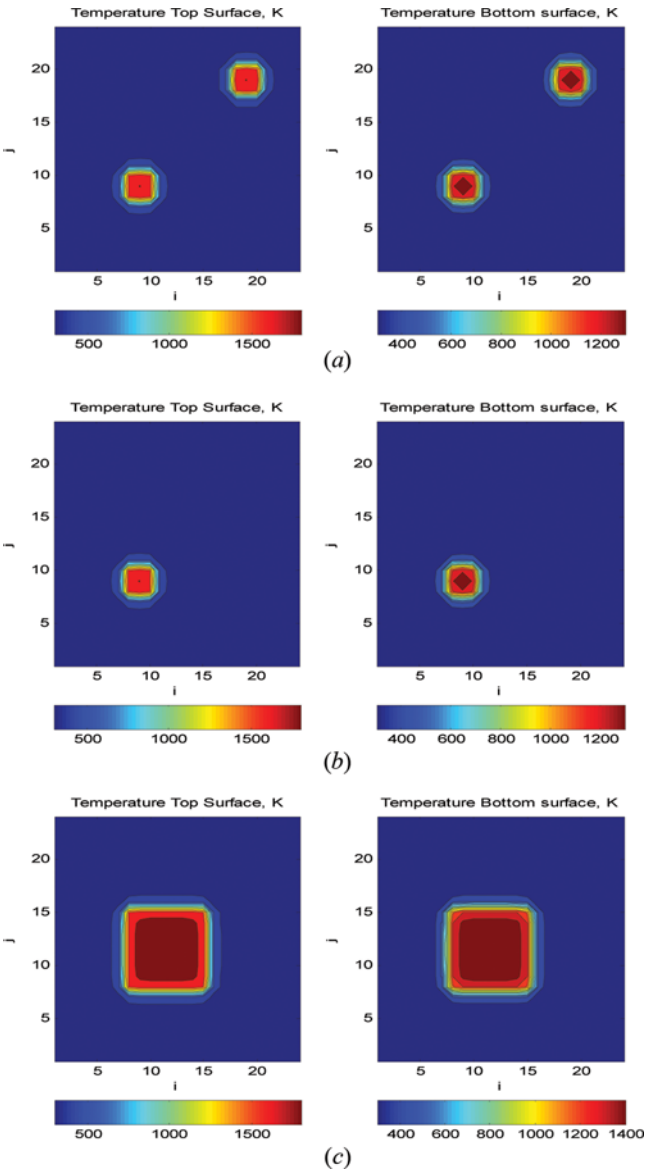

Figure 3. Temperatures at the bottom and top surfaces at $t = 1.9$ s for (*a*) heat flux A, (*b*) heat flux B, and (*c*) heat flux C (color figure available online).

2 K. On the other hand, the temperature measurements actually used in the inverse analysis, for the computation of the likelihood, were supposed to be more accurate, with standard deviations of 0.02 K or 1.25 K. From the means and variances of the local heat fluxes at each time step, 100 samples from a Gaussian distribution were generated for the spatially varying heat flux. The solutions of the complete and reduced models were then computed, in order to calculate the modeling

Table 1. Test cases

Test case	Flux	Prior	Approach
1	A	TV	–
2	B	TV	–
3	C	TV	–
4	A	TV	DAMH
5	B	TV	DAMH
6	C	TV	DAMH
7	A	Gaussian	–
8	B	Gaussian	–
9	C	Gaussian	–
10	A	Gaussian	AEM
11	B	Gaussian	AEM
12	C	Gaussian	AEM

error $\varepsilon(\mathbf{P}) = [\mathbf{T}_c(\mathbf{P}) - \mathbf{T}(\mathbf{P})]$, for each of these samples. Hence, the mean $\bar{\boldsymbol{\varepsilon}}$ and the covariance matrix $\mathbf{W}_\varepsilon$ were computed, to be used in the enhanced error model given by Eqs. (23*a*) and (23*b*).

In the inverse analysis, the numbers of states used in the Markov chains were 100,000 with 50,000 burn-in states and the proposal distribution $p(\mathbf{P}^*, \mathbf{P}^{(t-1)})$ was taken as Gaussian, with a standard deviation of $2 \times 10^{-3}\mathbf{P}^{(t-1)}$. For the hyperpriors, the center points of the Rayleigh distributions were taken as $\alpha_0 = 5 \times 10^{-4}\ \mathrm{mW}^{-1}$ for the TV prior and $\gamma_0 = 5 \times 10^{-4}$ for the Gaussian prior. Such quantities were selected based on numerical experiments and resulted in fast convergence of the Markov chains for all cases considered. This behavior is illustrated in Figure 4, which presents the evolution of the Markov chains of the heat fluxes at four different locations for case 3 with $\sigma = 0.02\,\mathrm{K}$. Note in this figure, that the chains converged for the actual values of the heat fluxes; that is, $10^7\ \mathrm{Wm}^{-2}$ for positions $i = j = 9$ and $i = j = 12$, and $0\ \mathrm{Wm}^{-2}$ for the other positions.

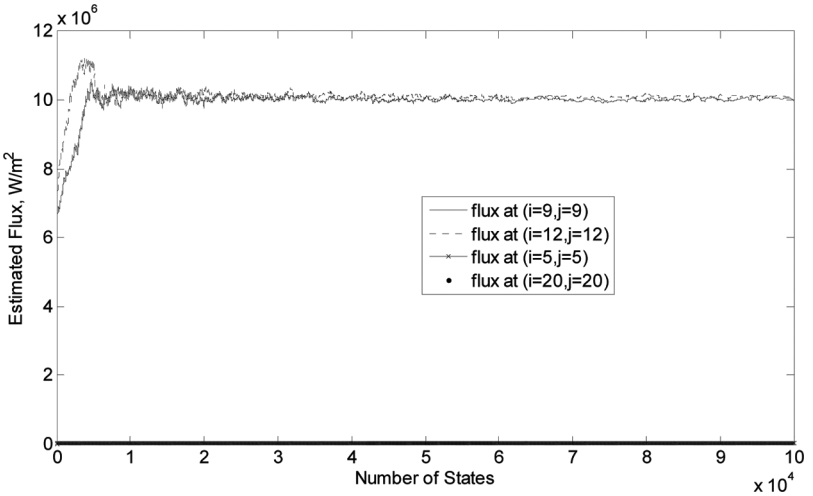

Figure 4. States of the Markov chains for four heat fluxes in test case 3 with $\sigma = 0.02\,\mathrm{K}$.

Table 2. CPU times, acceptance ratios, and RMS errors for measurements with standard deviation of $\sigma = 0.02\,\mathrm{K}$

Test case	CPU time (h)	Acceptance ratio (%)	RMS error (W/m^2)
1	2.7	10.9	9.3×10^4
2	2.8	9.0	6.6×10^4
3	2.6	9.9	1.1×10^5
4	114.2	46.7 – 5.3	9.8×10^4
5	113.0	47.9 – 4.2	5.9×10^4
6	98.3	40.8 – 5.9	1.4×10^5
7	2.6	11.3	9.3×10^4
8	2.8	9.3	6.6×10^4
9	2.7	10.2	1.1×10^5
10	44.5	12.8	4.1×10^4
11	44.2	11.0	2.6×10^4
12	42.5	11.2	8.5×10^4

The computational times for each of the test cases examined, together with the acceptance ratios and the RMS errors of the estimated heat fluxes, are presented in Table 2 for measurements with standard deviation of $\sigma = 0.02\,\mathrm{K}$. Similar results are presented in Table 3 for $\sigma = 1.25\,\mathrm{K}$. Both the acceptance ratios in the first test of Hastings with the reduced model (steps 2–4) and the second test of Hastings with the complete model (steps 5–7) are presented for cases 4–6, where the DAMH algorithm was applied. These ratios refer to the total number of states; that is, 100,000. The RMS error is defined as follows.

$$RMS_{error} = \sqrt{\frac{1}{IJ}\sum_{i=1}^{I}\sum_{j=1}^{J}\left[q_{exa}(x_i, y_j) - q_{est}(x_i, y_j)\right]^2} \tag{26}$$

Table 2 shows that the ratios of accepted states ranged between 9% and 12.8%, except for cases 4–6. For these cases, where the DAMH algorithm was used, the ratio of accepted states in the first test of Hastings was between 40% and 47%.

Table 3. CPU times, acceptance ratios, and RMS errors for measurements with standard deviation of $\sigma = 1.25\,\mathrm{K}$

Test case	CPU time (h)	Acceptance ratio (%)	RMS error (W/m^2)
1	2.6	9.1	1.1×10^6
2	2.6	7.5	1.0×10^6
3	2.6	9.1	1.8×10^6
4	98.7	41.9 – 6.8	1.1×10^6
5	93.5	44.6 – 5.7	6.9×10^5
6	64.5	34.6 – 5.4	1.4×10^6
7	2.7	9.1	1.1×10^6
8	2.6	8.3	9.8×10^5
9	2.6	9.4	1.3×10^6
10	42.9	9.8	1.2×10^6
11	43.3	11.9	1.2×10^6
12	43.1	8.7	2.0×10^6

However, around 90% of such accepted states were rejected in the second test of Hastings, when the complete model was applied. A comparison of test cases 1–3 with test cases 4–6 shows that the DAMH algorithm increased the acceptance ratio in the first test of Hastings, because samples accepted with the complete model better represented the actual components of the heat flux. On the other hand, the computational times substantially increased when the DAMH algorithm was used (cases 4–6), instead of the regular MH algorithm (cases 1–3), because the solution of the complete model for the direct problem needed to be computed for 40%–47% of the total states. Still, the computational times for the cases where the DAMH algorithm was used were approximately 50% of that expected if only the complete model was used for the inverse analysis; that is, 192 h. We also note that a further speed improvement could be done by an adaptive incorporation of knowledge about the approximation error in the DAMH algorithm, as demonstrated in reference [34]. The computational times were independent of the prior distribution, when only the reduced model was used in the inverse analysis (see cases 1–3 and 7–9). Similarly, the acceptance ratios were not significantly affected by the choice of the prior distribution. On the other hand, we also note a general increase on the computational times when the AEM approach was used (cases 10–12), as compared to the cases involving only the Gaussian prior (cases 7–9). This behavior resulted from matrix operations required for the computation of the posterior distribution with the AEM approach. An analysis of Table 2 reveals that the RMS errors were not affected by the choice of the prior distributions examined in this work, for measurements with standard deviation of $\sigma = 0.02\,\mathrm{K}$. Furthermore, the use of the DAMH algorithm (cases 4–6) did not improve the accuracy of the solution as compared to the regular MH algorithm (cases 1–3), but the use of the AEM approach (cases 10–12) reduced by approximately 50% the RMS errors with respect to cases 7–9, where only the Gaussian prior was applied with the reduced model.

The results obtained for measurements with standard deviation of $\sigma = 1.25\,\mathrm{K}$ are summarized in Table 3. Similar conclusions to those discussed above for measurements with standard deviation of $\sigma = 0.02\,\mathrm{K}$ (Table 2) can be drawn from the analysis of Table 3, with respect to the computational times and the acceptance ratios. On the other hand, it is interesting to note from the RMS errors in Table 3 that the accuracy of the inverse problem solution was not significantly improved or deteriorated, when the DAMH algorithm or the AEM approach were used instead of the reduced model. This behavior was due to the large standard deviations assumed for the measurements used in the cases presented in Table 3. Indeed, the RMS errors increased by around two orders of magnitude when the standard deviation of the measurement errors were increased from $\sigma = 0.02\,\mathrm{K}$ to $\sigma = 1.25\,\mathrm{K}$. Anyhow, the locations and the magnitudes of the applied heat fluxes can still be very well estimated even with such extremely large measurement errors, as will be apparent below.

A comparison of the estimated means and the exact applied heat fluxes is presented in Figures 5 and 6, for measurements with standard deviations of $\sigma = 0.02\,\mathrm{K}$ and $\sigma = 1.25\,\mathrm{K}$, respectively. The results presented in Figure 5 were obtained with the AEM approach (cases 10–12), while the results presented in Figure 6 were obtained with the DAMH algorithm (cases 4–6). Such figures illustrate the accuracy of these two techniques as applied to the solution of the present inverse problem. For the results obtained with measurements of small standard deviation,

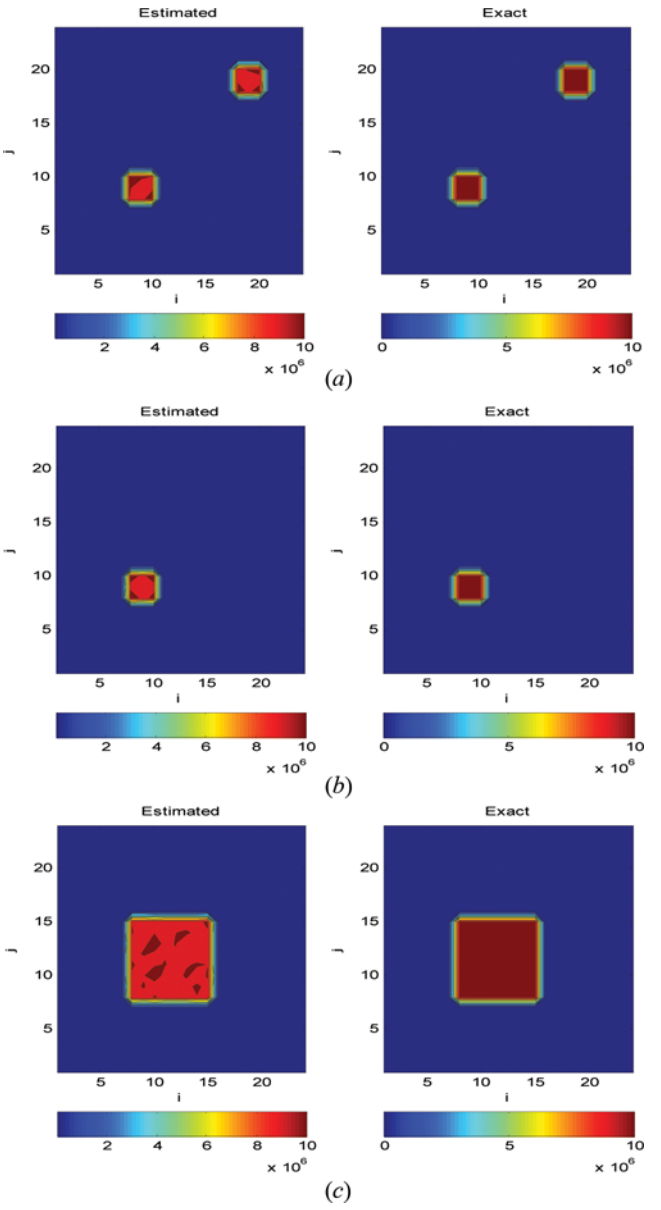

Figure 5. Estimated and exact heat fluxes for (*a*) case 10, (*b*) case 11, and (*c*) case 12 with $\sigma = 0.02\,\mathrm{K}$ (color figure available online).

we note that both the locations and the magnitudes of the applied heat fluxes were extremely well estimated, as depicted by Figure 5. Such is the case, despite the fact that a poor Gaussian prior, generated with measurements of large uncertainty as described above, was used for the results presented in this figure. An analysis of the results presented by Figure 6, which were obtained with measurements containing

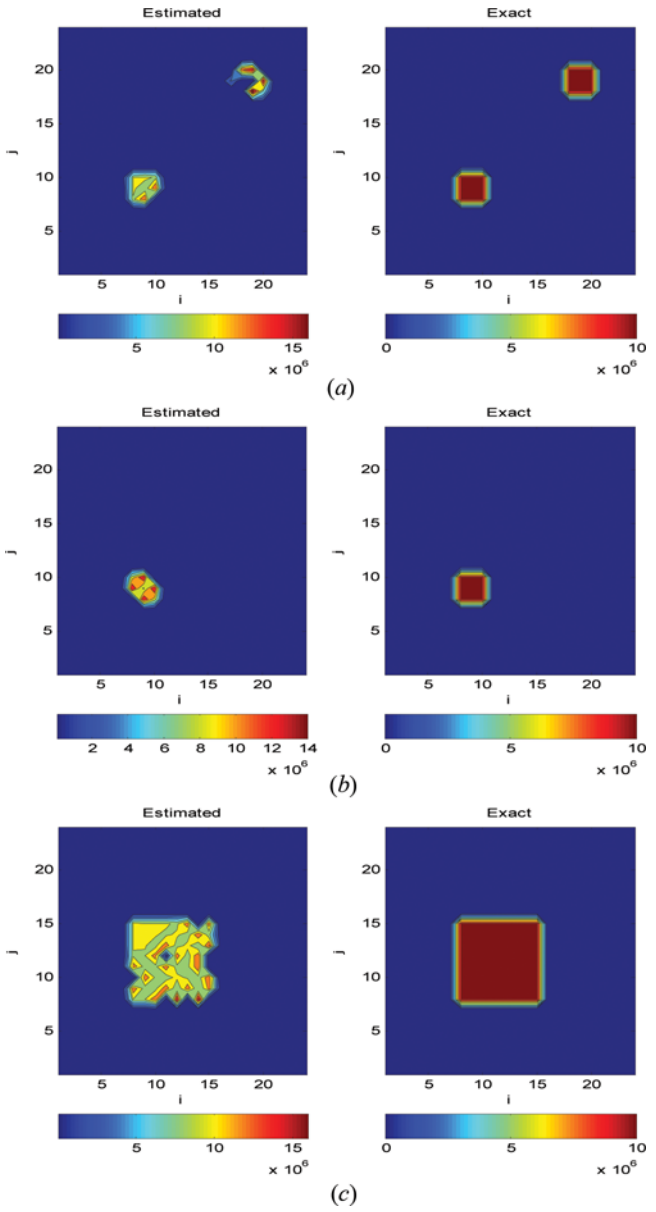

Figure 6. Estimated and exact heat fluxes for (*a*) case 4, (*b*) case 5, and (*c*) case 6 with $\sigma = 1.25\,\mathrm{K}$ (color figure available online).

errors of standard deviation $\sigma = 1.25\,\mathrm{K}$ by using the DAMH algorithm, shows that this technique was capable of accurately estimating the regions of the applied heat fluxes. Although oscillations can be observed within the regions where the heating was imposed, the estimated heat fluxes were stable and practically null, as expected, in regions where heat transfer was neglected (outside the heating spots). Such quite

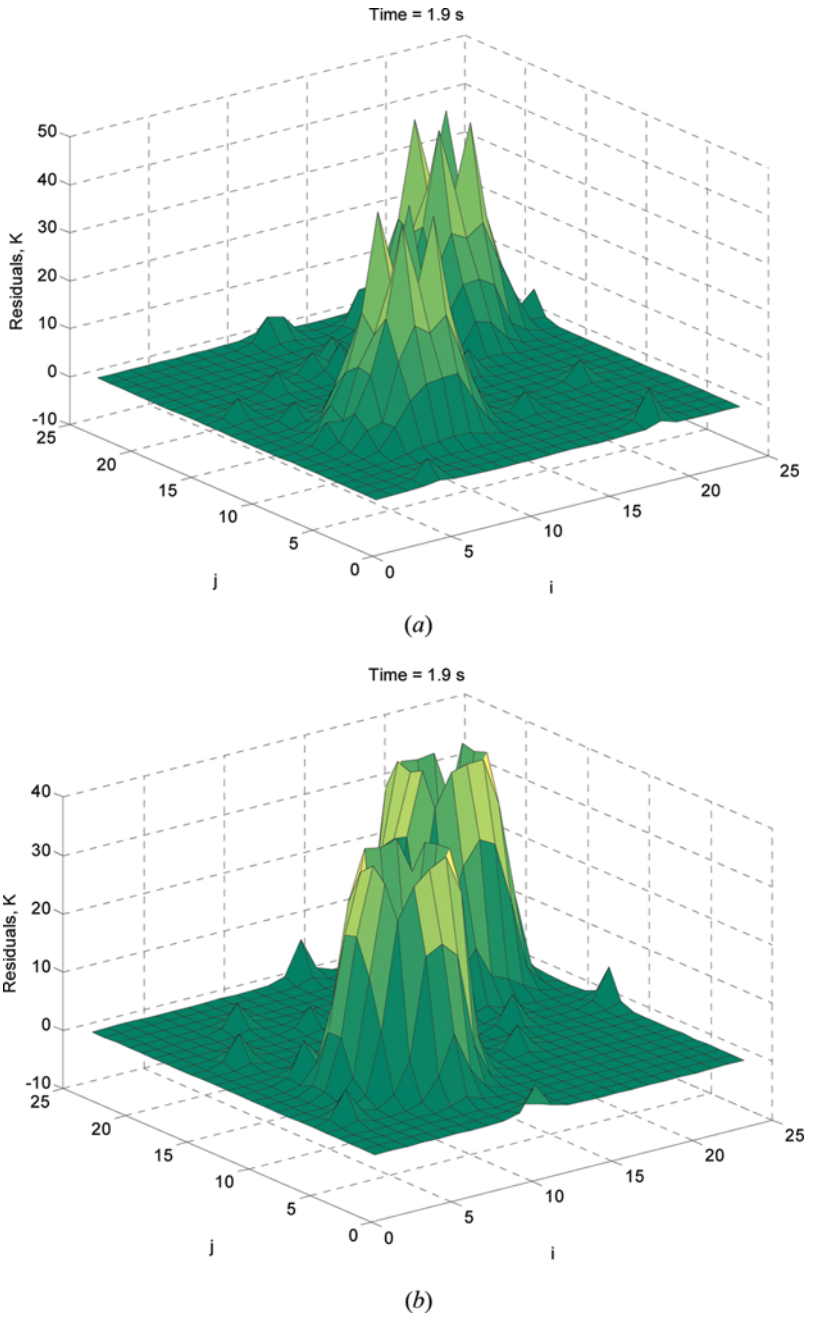

Figure 7. Residuals for (*a*) case 1 and (*b*) case 4 with $\sigma = 0.02$ K (color figure available online).

accurate results were obtained despite the very large measurement errors and with a prior that does not provide any information regarding the sought function, which is given in these cases by the total variation function.

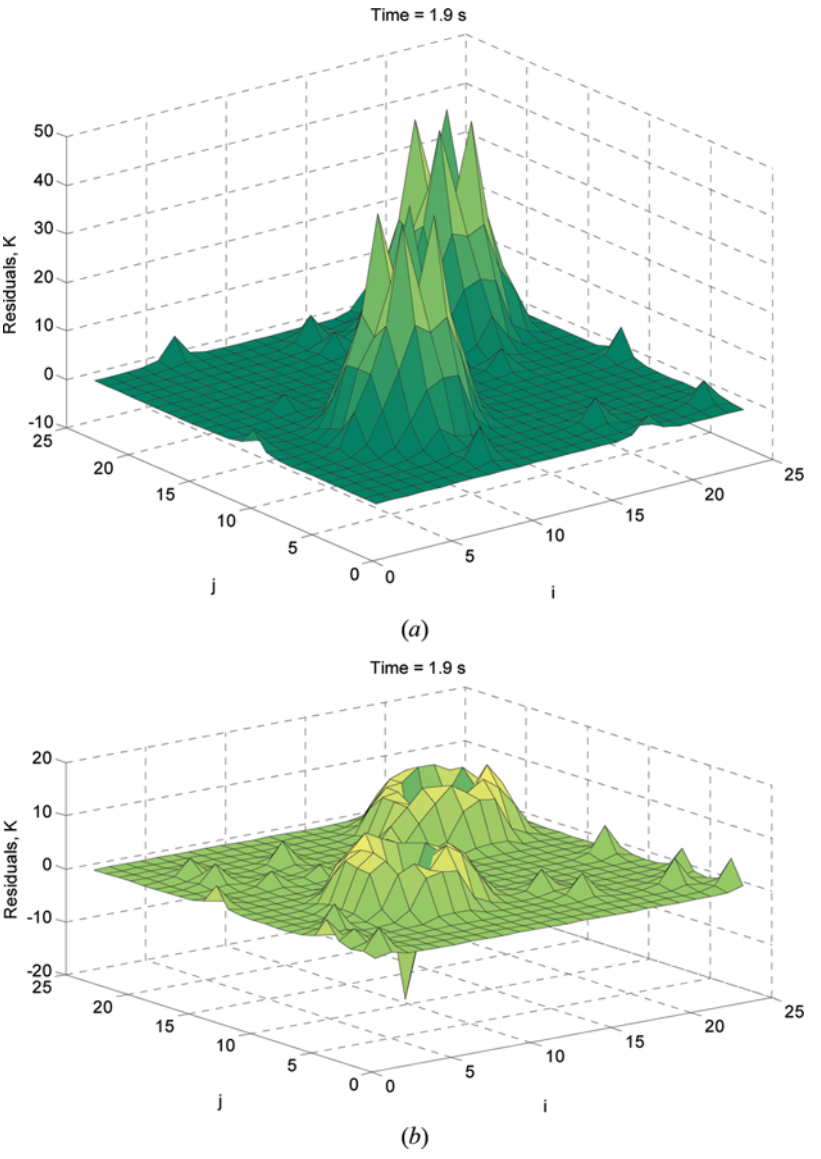

Figure 8. Residuals for (*a*) case 7 and (*b*) case 10 with $\sigma = 0.02\,\mathrm{K}$ (color figure available online).

Although the use of the DAMH algorithm did not result on significant changes on the accuracy of the estimated quantities (see Tables 2 and 3), we note that this algorithm actually samples from the correct complete model, thus providing a reduction on the temperature residuals. The residuals are defined as the difference between measured and estimated temperatures, where the last ones were calculated here with the complete model by using the estimated heat fluxes. Indeed, small and uncorrelated residuals are expected for the solution of inverse problems obtained with models that appropriately represent the physical phenomena of the

problem. Figure 7 presents the residuals at time $t = 1.9$ s for cases 1 and 4, respectively, for measurements with $\sigma = 0.02$ K. The time $t = 1.9$ s was selected for this analysis since it is close to the final time, where the residuals are larger than for small times. We note in this figure that the larger residuals take place at the edges of the regions where the heat flux was applied for case 4 (DAMH algorithm); while for case 1, which involves only the MH algorithm, the residuals are more evenly distributed within the heating regions and of larger magnitude. A reduction of the magnitude of the residuals was also noticed when the AEM approach was used, instead of only the reduced model with the Gaussian prior, as presented in Figure 8. Figure 8*a* shows the residuals for case 7 and Figure 8*b* shows the residuals for case 10, both for measurements with $\sigma = 0.02$ K, at time $t = 1.9$ s. It is interesting to note that Figures 7*a* and 8*a* present similar residuals when only the reduced model was used in the inverse analysis, for the two prior distributions examined in this paper. On the other hand, Figure 8*b* shows that the AEM approach was capable of significantly reducing the magnitude of the residuals and making them less correlated, for measurements with $\sigma = 0.02$ K, but such was not the case when the DAMH algorithm was applied (see Figure 7*b*). In fact, for measurements with $\sigma = 0.02$ K, the AEM approach also resulted in the smallest RMS errors as depicted by Table 2. The behavior of the residuals for measurements with $\sigma = 1.25$ K was practically not affected by the kind of prior distribution used for the inverse analysis; it was also not affected by the use of the DAMH algorithm or of the AEM approach, as a result of the extremely large standard deviation used for the simulated measurements in these cases. Such conclusions were already expected, based on the analysis of the RMS errors presented in Table 3.

CONCLUSION

In this article, the inverse problem dealt with the estimation of a boundary heat flux from transient measurements taken at the opposite surface, in a thin plate with temperature-dependent properties. The solution of the inverse three-dimensional nonlinear heat conduction problem was obtained with the Markov chain Monte Carlo method. A reduced model was used in this work, based on an improved lumped formulation of a linearized version of the complete model, in order to accelerate the inverse problem solution. Two prior distributions, as well as two approaches that aimed at improving the accuracy of the inverse problem solution with the reduced model, were examined in the paper. The priors analyzed for the heat flux included a total variation noninformative one, as well as a Gaussian that was modeled in terms of the physics of the problem. The approaches aimed at improving the accuracy of the inverse problem included the delayed Metropolis-Hastings (DAMH) algorithm and the approximation error model (AEM), in the form of the enhanced error model. Additive, Gaussian and uncorrelated simulated measurements were used in the inverse analysis, with two different levels of measurement errors. The solution of the inverse problem was examined for three different functional forms of the applied heat flux.

The two prior distributions examined here resulted on estimations of similar accuracy, for both levels of measurement errors, when only the reduced model

was used in the inverse analysis. For measurements with a large standard deviation, the behaviors of the residuals and of the RMS errors were practically not affected by the use of the DAMH algorithm or of the AEM approach. Anyhow, the locations and the magnitudes of the applied heat fluxes were very well estimated with large measurement errors, because of the careful selections of the prior distributions and of an accurate reduced model to replace the complete model. For measurements with small standard deviation, the AEM approach was capable of reducing the RMS errors of the estimated heat fluxes and resulting on less correlated residuals of smaller magnitudes. Although the DAMH algorithm did not effectively reduced the RMS errors for those measurements with smaller magnitudes, its residuals were also smaller and less correlated than those obtained with the sole application of the reduce model. In terms of the computational time, the DAMH algorithm resulted in a substantial increase as compared to the cases that dealt only with the reduced model, because the solution of the complete model needed to be computed for about 50% of the total states. Still, the computational times for the cases where the DAMH algorithm was used were approximately 50% of that expected if only the complete model was used in the analysis. An increase on the computational times was observed when the AEM approach was used, as compared to those obtained only with the reduced model, but the speed-up was of the order of four with respect to the solution of the inverse problem with the complete model.

This article demonstrates the importance of carefully selecting the reduced model for the solution of the direct problem, as well as the prior distributions for the unknown quantities, for an inverse analysis based on the Markov chain Monte Carlo method. For the cases examined herein, the use of the DAMH algorithm did not result in significant changes of the accuracy of the estimated quantities, although this algorithm actually samples from the correct complete model. On the other hand, the AEM approach, which uses the posterior modified by the error of the reduced model, allowed for an improvement on the accuracy of the inverse problem solution, for small experimental errors. Such was the case despite the fact that the AEM approach was based on a poor Gaussian prior, generated with a second set of measurements with large uncertainty.

REFERENCES

1. J. Kaipio and E. Somersalo, *Statistical and Computational Inverse Problems*, Applied Mathematical Sciences, 160, Springer-Verlag, 2004.
2. D. Gamerman and H. F. Lopes, *Markov Chain Monte Carlo: Stochastic Simulation for Bayesian Inference*, 2nd ed., Chapman & Hall/CRC, Boca Raton, FL, USA, 2006.
3. P. M. Lee, *Bayesian Statistics*, Oxford University Press, London, UK, 2004.
4. S. Tan, C. Fox, and G. Nicholls, *Inverse Problems*, Course Notes for Physics 707, University of Auckland, New Zealand, 2006.
5. J. Kaipio and C. Fox, The Bayesian Framework for Inverse Problems in Heat Transfer, *Heat Transfer Eng.*, vol. 32, pp. 718–753, 2011.
6. H. R. B. Orlande, Inverse Problems in Heat Transfer: New Trends in Solution Methodologies and Applications, *ASME J. of Heat Transfer*, vol. 134, p. 031011, 2012.
7. H. Orlande, O. Fudym, D. Maillet, and R. Cotta, *Thermal Measurements and Inverse Techniques*, CRC Press, Boca Raton, Florida, USA, 2011.

8. H. R. B. Orlande, M. J. Colaço, and G. S. Dulikravich, Approximation of the Likelihood Function in the Bayesian Technique for the Solution of Inverse Problems, *Inverse Problems in Sci. & Eng.*, vol. 16, pp. 677–692, 2008.
9. M. Neumayer, W. Watzenig, H. R. B. Orlande, M. J. Colaço, and G. Dulikravich, Fast Bayesian Inference for an Inverse Heat Transfer Problem using Approximations, *IEEE Int. Instrumentation and Measurement Technology Conference (I2MTC)*, Graz, 2012.
10. A. Ryfa, D. Ingham, and R. Bialecki, Direct and Inverse Methods for an Air Jet Impingement, *Numer. Heat Transfer A*, vol. 61, pp. 547–568, 2012.
11. J. Zhou, Y. Zhang, J. Chen, and Z. Feng, Inverse Estimation of Surface Temperature Induced by a Moving Heat Source in a 3-D Object Base on Back Surface Temperature with Random Measurement Errors, *Numer. Heat Transfer A*, vol. 61, pp. 85–100, 2012.
12. R. Chopade, S. Mishra, P. Mahanta, and S. Maruyama, Numerical Analysis of na Inverse Boundary Design Problem of a 3D Radiant Furnace with a 3-D Design Object, *Numer. Heat Transfer A*, vol. 60, pp. 25–49, 2011.
13. W.-Y. Chiou, C. Chen, and W. Lu, The Inverse Numerical Solutions of the Nonlinear Heat Transfer Problem in Electrical Discharge Machining, *Numer. Heat Transfer A*, vol. 59, pp. 247–266, 2011.
14. H. Molavi, I. Pourshaban, A. Hakkaki-Fard, M. Molavi, A. Ayasoufi, and R. Rahmani, Inverse Identification of Thermal Properties of Charring Ablators, *Numer. Heat Transfer B*, vol. 56, pp. 478–501, 2009.
15. M. Samai and T. Loulou, A Comparative Study of Heat Flux and Temperature Based Objective Functional to Solve Inverse Heat Conduction Problems, *Numer. Heat Transfer B*, vol. 56, pp. 75–104, 2009.
16. Y. Ren, Y. Zhang, J. Chen, and Z. Feng, Inverse Estimation of the Front Surface Temperature of a 3-D Finite Slab Based on the Back Surface Temperature Measured at Coarse Grids, *Numer. Heat Transfer B*, vol. 63, pp. 1–17, 2013.
17. A. Alsoy-Akgün and D. Lesnic, A Numerical Solution for an Inverse Natural Magneto-Convection Problem, *Numerical Heat Transfer B*, vol. 63, pp. 115–138, 2013.
18. A. Bensefia, M. Boussaid, and T. Loulou, Optimal Heat Input for Estimating Luikov's Parameters in a Heat and Mass Transfer Problem, *Numer. Heat Transfer B*, vol. 60, pp. 399–423, 2011.
19. H. Massard, O. Fudym, H. R. B. Orlande, and J. C. Batsale, Nodal Predictive Error Model and Bayesian Approach for Thermal Diffusivity and Heat Source Mapping, *Comptes Rendus Mécanique*, vol. 338, pp. 434–449, 2010.
20. H. Fonseca, H. R. B. Orlande, and O. Fudym, Estimation of Position-Dependent Transient Heat Source with the Kalman Filter, *Inverse Problems in Sci. and Eng.*, vol. 20, pp. 1079–1099, 2012.
21. C. Naveira-Cotta, H. Orlande, and R. Cotta, Combining Integral Transforms and Bayesian Inference in the Simultaneous Identification of Variable Thermal Conductivity and Thermal Capacity in Heterogeneous Media, *ASME J. of Heat Transfer*, vol. 133, pp. 111301–111311, 2011.
22. C. Naveira-Cotta, H. Orlande, and R. Cotta, Integral Transforms and Bayesian Inference in the Identification of Variable Thermal Conductivity in Two-Phase Dispersed Systems, *Numer. Heat Transfer B*, vol. 57, pp. 173–202, 2010.
23. C. Naveira-Cotta, R. Cotta, and H. Orlande, Inverse Analysis with Integral Transformed Temperature Fields: Identification of Thermophysical Properties in Heterogeneous Media, *Int. J. Heat and Mass Transfer*, vol. 54, pp. 1506–1519, 2011.
24. D. Knupp, C. Naveira-Cotta, R. Cotta, and H. Orlande, Experimental Identification of Thermophysical Properties in Heterogeneous Materials with Integral Transformation of Temperature Measurements from Infrared Thermography, *Exp. Heat Transfer*, vol. 26, pp. 1–25, 2013.

25. R. M. Cotta and M. D. Mikhailov, *Heat Conduction: Lumped Analysis, Integral Transforms, Symbolic Computation*, Wiley-Interscience, New York, USA, 1997.
26. D. Knupp, C. Naveira-Cotta, J. Ayres, R. Cotta, and H. Orlande, Theoretical-Experimental Analysis of Heat Transfer in Nonhomogeneous Solids via Improved Lumped Formulation, Integral Transforms and Infrared Thermography, *Int. J. Thermal Sciences*, vol. 62, pp. 71–84, 2012.
27. H. Orlande and H. Dulikravich, Inverse Heat Transfer Problems and their Solutions within the Bayesian Framework, *ECCOMAS Numerical Heat Transfer Conference*, pp. 1–18, Wroclaw, September 4–6, 2012.
28. J. Christen and C. Fox, Markov chain Monte Carlo using an Approximation, *J. of Computational and Graphical Statistics*, vol. 14, no. 4, pp. 795–810, 2005.
29. A. Nissinen, *Modelling Errors in Electrical Impedance Tomography*, Dissertation in Forestry and Natural Sciences, University of Eastern Finland, 2011.
30. A. Nissinen, L. Heikkinen, and J. Kaipio, The Bayesian Approximation Error Approach for Electrical Impedance Tomography—Experimental Results, *Meas. Sci. Tech.*, vol. 19, pp. 015501, 2008.
31. A. Nissinen, L. Heikkinen, V. Kolehmainen, and J. Kaipio, Compensation of Errors due to Discretization, Domain Truncation and Unknown Contact Impedances in Electrical Impedance Tomography, *Meas. Sci. Tech.*, vol. 20, pp. 105504, 2009.
32. A. Nissinen, V. Kolehmainen, and J. Kaipio, Compensation of Modeling Errors due to Unknown Boundary Domain in Electrical Impedance Tomography, *IEEE Trans. Med. Im.*, vol. 30, pp. 231–242, 2011.
33. A. Nissinen, V. Kolehmainen, and J. Kaipio, Reconstruction of Domain Boundary and Conductivity in Electrical Impedance Tomography using the Approximation Error Approach, *Int. J. Uncertainty Quant.*, vol. 1, pp. 203–222, 2011.
34. T. Cui, C. Fox, and M.J. O'Sullivan, *Adaptive Error Modelling in MCMC Sampling for Large Scale Inverse Problems*. Report (University of Auckland. Faculty of Engineering), Engineering Science, School of Engineering, University of Auckland, 2010.